Transp Porous Med (2010) 82:173–196
DOI 10.1007/s11242-009-9425-y

A Phase-Partitioning Model for CO_2–Brine Mixtures at Elevated Temperatures and Pressures: Application to CO_2-Enhanced Geothermal Systems

Nicolas Spycher · Karsten Pruess

Received: 8 December 2008 / Accepted: 1 June 2009 / Published online: 17 July 2009

Abstract Correlations are presented to compute the mutual solubilities of CO_2 and chloride brines at temperatures 12–300°C, pressures 1–600 bar (0.1–60 MPa), and salinities 0–6 m NaCl. The formulation is computationally efficient and primarily intended for numerical simulations of CO_2-water flow in carbon sequestration and geothermal studies. The phase-partitioning model relies on experimental data from literature for phase partitioning between CO_2 and NaCl brines, and extends the previously published correlations to higher temperatures. The model relies on activity coefficients for the H_2O-rich (aqueous) phase and fugacity coefficients for the CO_2-rich phase. Activity coefficients are treated using a Margules expression for CO_2 in pure water, and a Pitzer expression for salting-out effects. Fugacity coefficients are computed using a modified Redlich–Kwong equation of state and mixing rules that incorporate asymmetric binary interaction parameters. Parameters for the calculation of activity and fugacity coefficients were fitted to published solubility data over the *P–T* range of interest. In doing so, mutual solubilities and gas-phase volumetric data are typically reproduced within the scatter of the available data. An example of multiphase flow simulation implementing the mutual solubility model is presented for the case of a hypothetical, enhanced geothermal system where CO_2 is used as the heat extraction fluid. In this simulation, dry supercritical CO_2 at 20°C is injected into a 200°C hot-water reservoir. Results show that the injected CO_2 displaces the formation water relatively quickly, but that the produced CO_2 contains significant water for long periods of time. The amount of water in the CO_2 could have implications for reactivity with reservoir rocks and engineered materials.

Keywords CO_2 · Carbon dioxide · Solubility · Phase partitioning · Mutual solubility · Enhanced Geothermal System · EGS · Brine · Water Flow · Multiphase Flow

N. Spycher (✉) · K. Pruess
Lawrence Berkeley National Laboratory, MS 90-1116, 1 Cyclotron Road, Berkeley, CA, USA
e-mail: NSpycher@lbl.gov

1 Introduction

The burning of fossil fuels has become a serious concern because of associated CO_2 emissions and impacts on climate (IPCC 2005, 2008). As a result, many studies have been undertaken to assess the feasibility of CO_2 geologic storage as a mitigation measure to curb rising CO_2 emissions (IPCC 2005). Rising costs of fossil fuels have also led to a renewed interest in geothermal energy, and particularly in enhanced geothermal systems (EGS) (MIT 2006). With these systems, the recovery of heat from the subsurface is enhanced by water injection (e.g., Goyal 1995; Stark et al. 2005) and in some cases, water is injected, circulated, and recovered from areas that originally are dry or contain very little water (e.g., MIT 2006). The use of CO_2 instead of water as the heat transmission fluid in EGS has been proposed as a means not only to produce "clean" energy, but also to potentially sequester CO_2 through fluid losses at depth, which typically occur in any type of EGS (Brown 2000; Fouillac et al. 2004; Pruess 2006, 2008). Other potential advantages of CO_2-based EGS include increased heat extraction rates and wellbore flow compared to water-based systems, and lesser potential for unfavorable rock–fluid chemical interactions in engineered systems (Pruess 2006, 2008).

The solubility of CO_2 in water has obvious implications for long-term carbon sequestration and water–rock interactions (e.g., Gilfillan 2008; Moore et al. 2005; Rosenbauer et al. 2005; Palandri et al. 2005; Kaszuba et al. 2003). The solubility of water into CO_2 is also of importance, because it affects the reactivity of CO_2 with surrounding rocks (e.g., Regnault et al. 2005; Rimmelé et al. 2008; Lin et al. 2008; Suto et al. 2007) and determines the capacity of injected CO_2 to dry the rock formations adjacent to injection wells (Giorgis et al. 2007; Hurter et al. 2007; Pruess and Müller 2009). In the case of a CO_2-based EGS, the partitioning of water into CO_2 would also determine the time required for the removal of water from the (central portion of the) EGS, and the type of chemical interactions that may take place between the CO_2 plume, reservoir rocks, and engineered systems. Therefore, an important aspect in the study of CO_2 geologic storage and CO_2–EGS is the calculation of phase partitioning between CO_2 and formation waters.

At temperatures and pressures typically considered for geologic storage (<100°C and 200–400 bar), the mixing of CO_2 with water results in two immiscible phases, an H_2O-rich liquid phase and a CO_2-rich compressed "gas" phase (supercritical fluid) that contains only small amounts of water (typically <2 mol%; e.g., Spycher et al. 2003). At higher temperatures relevant to CO_2-based EGS, the same two-phase behavior persists, although the amount of water in the CO_2-rich phase increases significantly, reaching values of up to about 40–50 mol% at temperatures ~275°C and pressures between 200 and 600 bar (Takenouchi and Kennedy 1964, Todheide and Frank, 1964; Blencoe et al. 2001). At 300°C, water and CO_2 eventually become fully miscible at pressures above ~567 bar (Blencoe et al. 2001). The ability to compute this phase-partitioning behavior in a reliable and efficient manner is critical to predicting the flow of water and CO_2 in the subsurface using numerical models.

Several models have been proposed to compute the aqueous solubility of CO_2, with or without consideration of the water solubility in the CO_2 phase (see reviews by Hu et al. 2007; Spycher et al. 2003; Spycher and Pruess 2005 and references therein). However, most of these models are either too computationally intensive for their incorporation into efficient multiphase flow simulators, or consider only the solubility of CO_2 in water. We have previously developed a computationally efficient model to calculate the mutual solubilities of CO_2 and water from 12 to 100°C and up to 600 bar (Spycher et al. 2003). This model was later extended to chloride brines up to ~6 m NaCl over the same range of temperatures and pressures (Spycher and Pruess 2005). Here, motivated by the potential for CO_2–EGS and

CO_2 geologic storage at temperatures above 100°C, this mutual solubility model is extended to temperatures up to 300°C.

2 Phase-Partitioning Model

2.1 Model Formulation (CO_2–H_2O System)

Our original model (Spycher et al. 2003) was intended for temperatures ≤100°C, at which two assumptions held reasonably well when calculating activity and fugacity coefficients: unit activity coefficients for liquid water and aqueous CO_2 in pure water, and infinite water dilution in the compressed CO_2 phase. At higher temperatures, these assumptions start to fail because the mutual solubilities of CO_2 and water increase significantly. Therefore, for applications at temperatures >100°C, an activity coefficient model for liquid water and aqueous CO_2 was implemented, and mixing rules for the equation of state were revised as described below. The extended model formulation is such that a smooth transition can be obtained from the original model at temperatures ≤100°C to higher temperatures. The model formulation is summarized below and in Appendices A and B, with parameters listed in Table 1. Additional details can be found in Spycher et al. (2003).

The equilibrium between water and CO_2 is expressed by two reactions

$$H_2O_{(l)} <==> H_2O_{(g)} \quad K_{H_2O} = f_{H_2O(g)}/a_{H_2O(l)} \tag{1}$$

$$CO_{2(aq)} <==> CO_{2(g)} \quad K_{CO_2(g)} = f_{CO_2(g)}/a_{CO_2(aq)} \tag{2}$$

each with an equilibrium constant K defined in terms of fugacities (f) for gaseous H_2O and CO_2, and activities (a) for aqueous CO_2 and liquid water. Note that the subscript (g) refers to the CO_2-rich phase, which for CO_2 may be either gaseous, liquid, or supercritical, but for simplicity, will henceforth be referred to as "gas." Values of K depend only on temperature and pressure. The departure from ideality, including concentration effects, is taken into account by activity coefficients (γ) for aqueous species and liquid water, and fugacity coefficients (Φ) for gaseous species, with the convention that

$$a_i = \gamma_i m_i \text{ (on a molality scale)} \quad \text{or} \quad a_i = \gamma_i x_i \text{ (on a mole-fraction scale)} \tag{3}$$

and

$$f_i = \Phi_i p_i = \Phi_i y_i P \tag{4}$$

where i designates the component in the mixture (CO_2 or H_2O), m stands for molality, x and y are the mole fractions in the aqueous and compressed gas phases, respectively, p is the gas partial pressure, and P is the total pressure. By convention, K is expressed using f values defined with respect to a reference state fugacity of 1 bar, and with values of a defined on a mole fraction scale for water and a molality scale for aqueous CO_2 (e.g., Denbigh 1983). Equilibrium constants defined in this way are computed as functions of temperature and pressure using the following relationships:

$$K_{(T,P)} = K^0_{(T,P_{\text{ref}})} \exp\left(\frac{(P - P_{\text{ref}})\overline{V}}{RT_{\text{k}}}\right) \tag{5}$$

with $\log(K^0)_{T,P_{\text{ref}}}$ and P_{ref} expressed as functions of temperature

$$F(T) = a + bT + cT^2 + dT^3 + eT^4 \tag{6}$$

Table 1 Parameters for the CO_2–H_2O mutual solubility model

Parameter	Equations	Parameter units	Regression coefficients				
			a	*b*	*c*	*d*	*e*
Low-temperature parameters: 12–109°C, 1–600 bar (Spycher et al. 2003)							
a_{CO_2}	A-3, A-8, A-7	bar cm^6 K$^{0.5}$ mol^{-2}	7.54×10^7	-4.13×10^4			
a_{H_2O}[a]	A-3, A-8, A-7	bar cm^{6}K$^{0.5}$ mol^{-2}	0.0	0.0			
$a_{CO_2-H_2O}$	A-3, A-8, A-7	bar cm^6 K$^{0.5}$ mol^{-2}	7.89×10^7	0.0			
b_{CO_2}	A-4, A-8, A-7	cm^3 mol^{-1}	27.80				
b_{H_2O}	A-4, A-8, A-7	cm^3 mol^{-1}	18.18				
$\log(K^0_{H_2O})$	5, 6	bar	–2.209	3.097×10^{-2}	-1.098×10^{-4}	2.048×10^{-7}	0.0
$\log(K^0_{CO_2})(L)$[b]	5, 6	bar mol^{-1}	1.169	1.368×10^{-2}	-5.380×10^{-5}	0.0	0.0
$\log(K^0_{CO_2})$	5, 6	bar mol^{-1}	1.189	1.304×10^{-2}	-5.446×10^{-5}	0.0	0.0
$\overline{V}_{CO_2}$	5, 7	cm^3 mol^{-1}	32.6	0.0			
$\overline{V}_{H_2O}$	5, 7	cm^3 mol^{-1}	18.1	0.0			
A_M	12 – 15	NA	0.0	0.0			
P_{ref}	5, 6	bar	1.0	0.0	0.0	0.0	0.0
High-temperature parameters: 99 – 300°C, 1–600 bar (this study, from data listed in Table 2)							
a_{CO_2}	A-3, A-8, A-7	bar cm^6 K$^{0.5}$ mol^{-2}	8.008×10^7	-4.984×10^4	0.0	0.0	0.0
a_{H_2O}	A-3, A-8, A-7	bar cm^6 K$^{0.5}$ mol^{-2}	1.337×10^8	-1.4×10^4	0.0	0.0	0.0
$a_{CO_2-H_2O}$	A-3, A-8, A-7	bar cm^6 K$^{0.5}$ mol^{-2}	Computed from $K_{H_2O-CO_2}$ and $K_{CO_2-H_2O}$ below				
$K_{H_2O-CO_2}$	A-6, A-7	NA	1.427×10^{-2}	-4.037×10^{-4}			
$K_{CO_2-H_2O}$	A-6, A-7	NA	0.4228	-7.422×10^{-4}			
b_{CO_2}	A-4, A-8, A-7	cm^3 mol^{-1}	28.25				
b_{H_2O}	A-4, A-8, A-7	cm^3 mol^{-1}	15.70				
$\log(K^0_{H_2O})$	5, 6	bar	–2.1077	2.8127×10^{-2}	-8.4298×10^{-5}	1.4969×10^{-7}	-1.1812×10^{-10}
$\log(K^0_{CO_2})$	5, 6	bar mol^{-1}	1.668	3.992×10^{-3}	-1.156×10^{-5}	1.593×10^{-9}	0.0
$\overline{V}_{CO_2}$	5, 7	cm^3 mol^{-1}	32.6	3.413×10^{-2}			
$\overline{V}_{H_2O}$	5, 7	cm^3 mol^{-1}	18.1	3.137×10^{-2}			

Table 1 continued

Parameter	Equations	Parameter units	Regression coefficients				
			a	*b*	*c*	*d*	*e*
A_M	12–15	NA	-3.084×10^{-2}	1.927×10^{-5}			
P_{ref} (T ≤ 100°C)	5,6	bar	1.0	0.0	0.0	0.0	0.0
P_{ref} (T > 100°C)[c]	5, 6	bar	-1.9906×10^{-1}	2.0471×10^{-3}	1.0152×10^{-4}	-1.4234×10^{-6}	1.4168×10^{-8}
CO_2 activity coefficient for salt effects: ~20 − 305°C (this study, from data listed in Table 3)							
λ	18, 19	NA	2.217×10^{-4}	1.074	2648		
ξ	18, 19	NA	1.30×10^{-5}	−20.12	5259		

[a] A value of a_{H_2O} is not needed because of the assumption of $y_{H_2O} = 0$ in mixing rules

[b] For liquid CO_2 below 31°C and above CO_2 saturation pressures

[c] Water saturation pressure

and

$$\overline{V} = a + b(T_K - 373.15) \quad \text{and} \quad b = 0 \text{ at } T_K < 373.15\,K \tag{7}$$

where T is the temperature in degrees Celsius, T_K is the temperature in degrees Kelvin, P is the total pressure of the system in bar, and P_{ref} is a reference pressure, here taken as 1 bar up to 100°C, and as the pure water saturation pressure above 100°C. R is the gas constant, and $\overline{V}$ is the average partial molar volume of the pure condensed phase (CO_2 or water) over the pressure interval P_{ref} to P. Coefficients a through e are regression coefficients that can express, as needed, the non-linearity in Gibbs free energy and $\overline{V}$ changes with temperature at constant pressure.

The mutual solubilities of water and CO_2 are then expressed as follows:

$$y_{H_2O} = A(1 - x_{CO_2}) \tag{8}$$

$$x_{CO_2} = B(1 - y_{H_2O}) \tag{9}$$

with parameters A and B defined as (using values of K given by Eqs. 5–7)

$$A = \frac{K_{H_2O}\gamma_{H_2O}}{\Phi_{H_2O} P_{tot}} \tag{10}$$

$$B = \frac{\Phi_{CO_2} P_{tot}}{55.508\ \gamma_{CO_2} K_{CO_2}} \tag{11}$$

Note that in these expressions, the activity coefficients γ_{H_2O} and γ_{CO_2} are both defined on a mole fraction scale, although K_{CO_2} is still defined on a molality scale. At temperatures ≤100°C and pressures of interest (up to 600 bar), the solubility of CO_2 in water is limited, such that a satisfactory accuracy is obtained by assuming $\gamma_{H_2O} = 1$ and $\gamma_{CO_2} = 1$. At higher temperatures, however, the CO_2 solubility in water increases significantly and unit activity coefficients can no longer be assumed. For this reason, for application at temperatures >100°C, an activity coefficient model needs to be implemented. This is done here using Margules expressions that were modified after Carlson and Colburn (1942) to yield unit activity coefficients for pure water ($\gamma_{H_2O} \to 1$ as $x_{H_2O} \to 1$) and for pure CO_2 at infinite dilution ($\gamma_{CO_2} \to 1$ as $x_{CO_2} \to 0$). These expressions obey the Gibbs–Duhem equation and take the following form:

$$\ln(\gamma_{H_2O}) = (A_M - 2A_M x_{H_2O}) {x_{CO_2}}^2 \tag{12}$$

$$\ln(\gamma_{CO_2}) = 2A_M x_{CO_2} {x_{H_2O}}^2 \tag{13}$$

In these equations, A_M is a Margules parameter that, after several tests, we chose to express as a function of temperature, as follows:

$$A_M = 0 (\text{thus } \gamma_{CO_2} \text{ and } \gamma_{H_2O} = 1) \quad \text{at } T \le 100°C \tag{14}$$

$$A_M = a(T_K - 373.15) + b(T_K - 373.15)^2 \quad \text{at } T > 100°C \tag{15}$$

Note that within our P–T range of interest, values of γ_{H_2O} remain very close to 1, although this is not the case for γ_{CO_2} at elevated CO_2 concentrations.

The fugacity coefficients Φ_{H_2O} and Φ_{CO_2} are computed using a modified Redlich–Kwong equation of state (Appendix A) that is unchanged from Spycher et al. (2003). However, for applications at temperatures >100°C, the mixing rules for this equation of state were expanded to include asymmetric binary interaction parameters (Panagiotopoulos and Reid 1986) as described in Appendix A. Below 100°C, the binary interaction parameters are ignored (set to 0), and the mixing rules revert to their original form.

2.2 Numerical Implementation

At temperatures below 99°C, the model is applied using the low-temperature parameters in Table 1, which are unchanged from those of Spycher et al. (2003). In this case, Eqs. 8 and 9 are solved by substitution, yielding

$$y_{H_2O} = (1 - B)/(1/A - B) \tag{16}$$

Once y_{H_2O} is obtained from Eq. 16, x_{CO_2} is recovered with Eq. 9. The cubic equation of state (Eq. A-2) is solved directly (Nickalls 1993). Also, y_{H_2O} is set to 0 in Eqs. A-3 through A-6 and A-8, and Eq. 14 yields unit activity coefficients (assumption of infinite dilution of water in CO_2 and of CO_2 in water). As a result, the mutual solubilities are computed in a direct manner without recourse to an iterative procedure.

At temperatures >109°C, the model is applied using the high-temperature parameters in Table 1. Because infinite dilution can no longer be assumed (i.e., $y_{H_2O} \neq 0$ in mixing rules, $\gamma_{H_2O} \neq 1$ and $\gamma_{CO_2} \neq 1$), an iterative procedure is required to solve Eqs. 8 and 9. This is accomplished at a small computational cost by using Eq. 16 and simple back-substitution. Because Eq. 16 is already substituted, iterating and back-substituting y_{H_2O} in the A and B terms of this equation was found to be both computationally faster and more robust than a full Newton–Raphson procedure with Eqs. 8 and 9. Satisfactory convergence is obtained by assuming initial $y_{H_2O} = P_{sat_{(H_2O)}}/P$ (ideal mixing), and initial $x_{CO_2} \approx 0.009$ (a concentration of ~0.5 molal).

At temperatures between 99 and 109°C, the results of both high-temperature and low-temperature calculations are blended by weighting linearly the fugacity coefficient values (Eq. A-8) and equilibrium constants (Eq. 6) obtained using both sets of parameters in Table 1. By blending model parameters rather than results, a smooth transition is obtained from the low-temperature noniterative model to the high-temperature iterative model.

2.3 Salt Effects

The model is extended to saline solutions by including the effect of dissolved salts in the activity coefficients that appear in Eqs. 10 and 11. Here, for convenience, we keep the activity coefficient model for the pure-water system unchanged (i.e., Eqs. 12 and 13 remain unchanged, with mole fractions defined on a salt-free basis). A separate activity coefficient (γ'_{CO_2}) for the salting out of CO_2 is introduced into Eq. 11, which becomes

$$B' = \frac{\Phi_{CO_2} P_{tot}}{55.508 \gamma_{CO_2} \gamma'_{CO_2} K_{CO_2}} \tag{17}$$

We have previously reviewed several activity coefficient models to compute values of γ'_{CO_2} (Spycher and Pruess 2005), and highlighted the Pitzer models adopted by Rumpf et al. (1994) and Duan and Sun (2003), which are essentially similar although formulated somewhat differently. We also pointed out that the activity coefficient model of Duan and Sun (2003) does not yield "true" activity coefficients (because of model simplifications regarding the gas phase), but instead gives the ratio of CO_2 concentrations in pure and saline water. As such, we previously used, as-is, the activity coefficient expression and parameters of Duan and Sun to compute the CO_2 solubility in saline water from its solubility in pure water (Spycher and Pruess 2005). This approach, however, is no longer applicable at elevated temperatures and pressures, where single-phase behavior (full miscibility) may occur for the pure-water system, but two-phase behavior prevails for the saline system at the same temperatures and pressures. Furthermore, Duan and Sun's model was not intended for temperatures

above about 260°C for the pure-water system, leading to significant deviations at 300°C. Nevertheless, the Pitzer expression of Duan and Sun and their useful simplification for salts other than NaCl is quite practical. For this reason, we adopt their formulation, but re-parameterize it to yield values of γ'_{CO_2} suitable for Eq. 17 and our *P–T* range of interest. After converting their Pitzer expression to a (CO_2-free) mole-fraction scale, we obtain:

$$\gamma'_{CO_2} = \left(1 + \frac{\sum m_{i\neq CO_2}}{55.508}\right) \exp\{2\lambda(m_{Na} + m_K + 2m_{Ca} + 2m_{Mg}) + \xi m_{Cl}(m_{Na} + m_K + m_{Ca} + m_{Mg}) - 0.07\, m_{SO_4}\} \quad (18)$$

where m stands for aqueous molalities, and $\gamma'_{CO_2} \rightarrow 1$ as the total concentration of dissolved salts tends to 0. Note that the first term in this expression is the conversion factor from molality to mole-fraction scale. Parameters λ and ξ are coefficients that can be defined as functions of temperature and pressure. However, a pressure dependence was neglected, because allowing for it did not improve the overall model accuracy over the *P–T* range of interest here. Satisfactory results were obtained using the following function of temperature, which is similar in type to that used by Rumpf et al. (1994):

$$F(T_K) = a\, T_K + b/T_K + c/T_{K^2} \quad (19)$$

It should be noted that because γ'_{CO_2} is defined independently of the aqueous CO_2 concentration, it can be computed externally to the iterations required (at elevated temperatures) to solve for mutual solubilities.

As before, the effect of salt on water activity is treated by assuming equality of water activity and mole fraction, which is a reasonable approximation up to halite saturation (Spycher and Pruess 2005). Therefore, an additional activity coefficient for the salt effect on water is not required as for the case of aqueous CO_2. In doing so, no changes are required in Eq. 10, and mutual solubilities are computed using modified forms of Eqs. 16 and 9 as described in Appendix B.

2.4 Model Parameterization and Results

Model parameters (Table 1) were optimized by fitting the mutual solubility model to available data using PEST (Doherty 2008). For calculations below 99°C, parameters and results for the pure-water system were unchanged from those of our previous work (Spycher et al. 2003), and rely on data sources listed therein. For calculations at higher temperatures, and salting-out effects at all temperatures, parameters were determined as part of this study using data from various literature sources, as described below.

Redlich–Kwong parameters were fitted using compressibility factors from Span and Wagner (1996) for pure CO_2, and Wagner and Pruss (2002) for pure H_2O. We also used the reference data from Wagner and Pruss (2002) to regress values of $K^0_{H_2O}$ (which are equal to the fugacity of pure water) and water saturation pressures as functions of temperature. Once these parameters were determined, other parameters for the pure-water system were obtained by inverting the full model to experimental mutual solubilities for the CO_2–H_2O system (Table 2). Once all the parameters for the pure-water system were determined, the model was inverted to experimental CO_2 solubilities in saline solutions (Table 3) to yield parameters for γ'_{CO_2} (Eqs. 18 and 19).

Model results for pure water and CO_2 from 12°C to 100°C and up to 600 bar were presented previously (Spycher et al. 2003), showing agreement with experimental data typically within the range of data uncertainty. The model, as extended here to higher temperatures, also performs reasonably well (Figs. 1 and 2). The computed aqueous CO_2 concentrations

Table 2 Experimental studies used for the parameterization of the high-temperature CO_2–H_2O mutual solubility model

Authors	Fitted T range (°C)	Fitted P range (bar)
Wiebe and Gaddy (1939)	100	25–405
Gillepsie and Wilson (1982)	93–260	7–203
Sako et al. (1991)	148	102–197
Malinin and Kurovskaya (1975)	100,150	48
Müller et al. (1988)	100–200	3–81
Takenouchi and Kennedy (1964)	110–300	100–600
Takenouchi and Kennedy (1965)	150–300	100–600
Coan and King (1971)	100	37–52
Drummond (1981)	100–305	58–195
Blencoe et al. (2001)	300	276–567
Nighswander et al. (1989)	120–198	21–102
Malinin (1959)	200–300	98–588
Shagiakhmetov and Tarzimanov (1981)	100,150	100–600
Tödheide and Frank (1963)	100–300	200–600

For many studies, the range of experimental conditions extends beyond the range listed here for the conditions of interest

Table 3 Experimental studies used for the parameterization of activity coefficients for saline solutions

Authors	Fitted T range (°C)	Fitted P range (bar)	Salt
Koschel et al. (2006)	50–100	50–202	1–3 m NaCl
Bando et al. (2003)	30–60	100–200	0.17–0.53 m NaCl
Kiepe et al. (2003)	40–80	2–101	0.52–4.3 m NaCl
Rumpf et al. (1994)	40–160	1.5–96	4–6 m NaCl
Nighswander et al. (1989)	80	23–102	0.18 m NaCl
Gehrig et al. (1986)[a]	212–321	125–603	1.1 m NaCl
Cramer (1982)	25–144	8–21	0.5–2 m NaCl
Drummond (1981)	20–305	35–206	1–6 m NaCl
Malinin and Kurovskaya (1975)	25–100	48	0.36–5.9 m NaCl
Malinin and Savelyeva (1972)	20–100	48	0.44–6 m $CaCl_2$
Takenouchi and Kennedy (1965)	150–300	100–600	1.1–4.3 m NaCl
Prutton and Savage (1945)	76–121	15–610	1.1–4 m $CaCl_2$
Markham and Kobe (1941)	24–40	1	1–4 m NaCl

For many studies, the range of experimental conditions extends beyond the range listed here for the conditions of interest

[a] Excluding points above 4 mol% CO_2 in the critical region

fall within a narrow scatter of experimental data points, with a root mean square difference (RMSD[1]) of about 7% (left side of Figs.1 and 2). Note that at 300°C, the dew point data of Blencoe et al. (2001) are well reproduced up to pressures of about 500 bar, above which the model reliability should be questioned as full miscibility is approached (according to Blencoe et al. 2001, the critical line at 300°C occurs at about 567 bar). Note that at 300°C and pressures above 500 bar, the CO_2 solubilities measured by Blencoe et al. (2001) agree well with those determined by Takenouchi and Kennedy (1964), but differ significantly from the measurements of Tödheide and Frank (1963). Blencoe et al. (2001) discussed at length the discrepancies between the results of these authors, and evaluated potential reasons for these discrepancies. On one hand, equilibrium could have been more closely approached in the

[1] Here, RMSD is defined as the square root of the average of all the squared differences (in percent) between the observed and measured data.

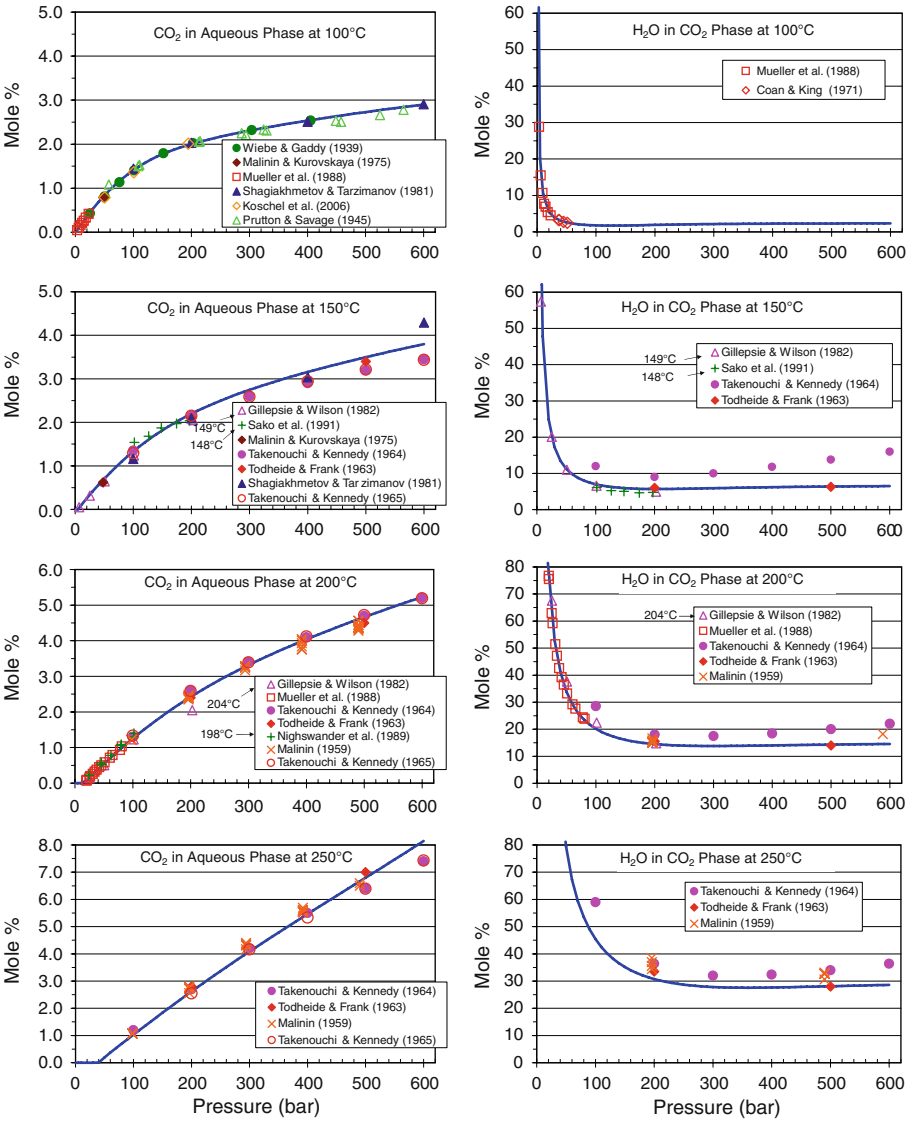

Fig. 1 Mutual solubilities of CO_2 and pure water: Comparison of model results (*lines*) with experimental data (*symbols*) from 100 to 250°C up to 600 bar

experiments performed by Todheide and Frank, because their mixtures were mechanically mixed but those of Takenouchi and Kennedy were not. On the other hand, the experimental procedures of Todheide and Frank could have been more amenable to water loss than the procedures of Takenouchi and Kennedy. In this article, we make no attempt to resolve these discrepancies, except to point out below that the gas-phase data of Todheide and Frank appear more consistent with other studies.

The computed water solubilities in compressed CO_2 yield a larger RMSD of about 17%, in large part due to the noticeable divergence between the gas-phase data reported by Tödheide

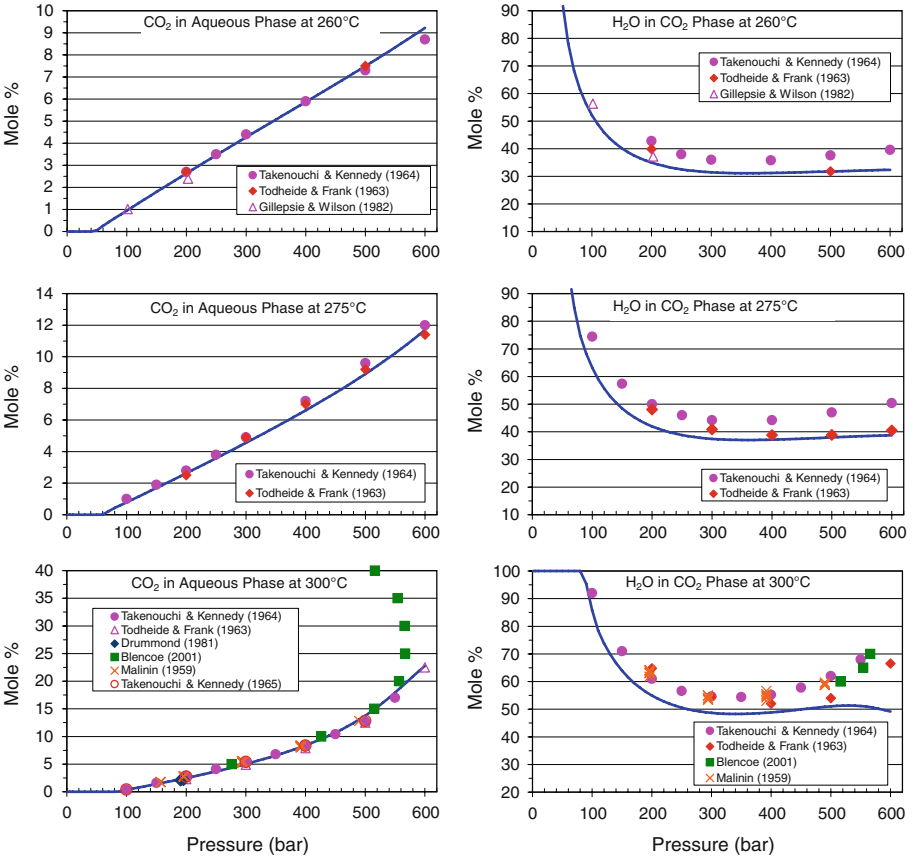

Fig. 2 Mutual solubilities of CO_2 and pure water: Comparison of model results (*lines*) with experimental data (*symbols*) above 250°C up to 300°C and 600 bar. Note that at 300°C, the model starts to break down above about 500 bar, as full miscibility is approached (the critical curve at 300°C is reached at around 567 bar; Blencoe et al. 2001)

and Frank (1963) and Takenouchi and Kennedy (1964, 1965) (right side of Figs. 1 and 2). The latter are not reproduced very well, and the model appears in much better agreement with the water solubilities determined by Tödheide and Frank (1963). At and below 260°C, the data of Todheide and Frank display a good continuity with the water solubilities measured at lower pressures by Müller et al. (1988) and Gillepsie and Wilson (1982). This would suggest that the gas-phase data of Todheide and Frank may be more accurate than those reported by Takenouchi and Kennedy. At 300°C, the model appears to somewhat underestimate the amount of water in CO_2, with results still closer to the measurement of Todheide and Frank than those of Takenouchi and Kennedy. The model eventually completely deviates from the measured trend above 500 bar as fully miscible behavior is approached.

Compressibility factors for pure CO_2 and pure water between 100 and 300°C and up to 600 bar are reproduced with RMSD values of about 0.5% and 0.2%, respectively. For mixtures, the model also appears to yield reasonable values for the volume of the compressed gas phase, although only limited volumetric data are available for comparisons in our *P–T* range of interest (Fig. 3).

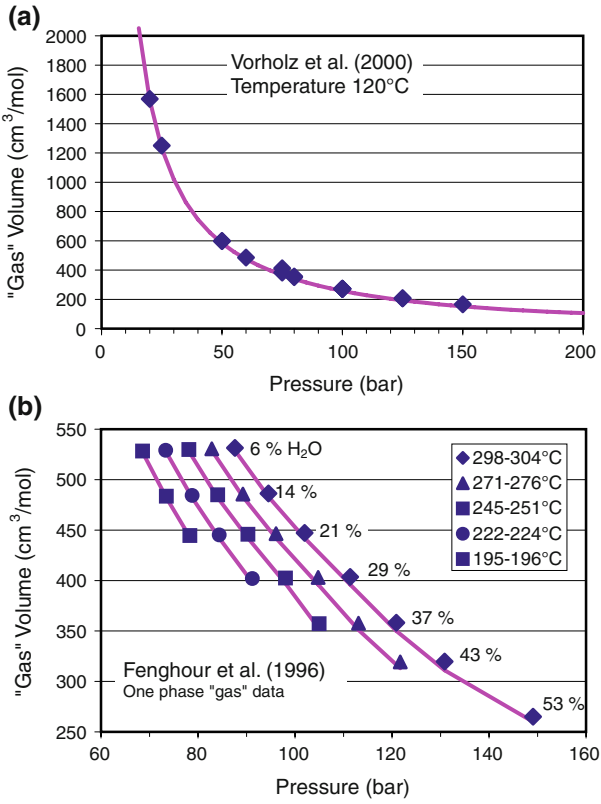

Fig. 3 Volume of the compressed "gas" phase for mixtures of CO_2 and pure water. Comparison of model results (*lines*) with data from other sources (*symbols*): (**a**) volumes at the phase boundary determined from molecular simulations; (**b**) experimental data for various water contents, near and progressively away from the phase boundary

For saline solutions, the experimental CO_2 solubility data in Table 3 are reproduced with an RMSD value of about 7% (Fig. 4). Our model also agrees within similar margins with the model of Duan and Sun (2003) (Fig. 5), which is intended for a wider *P–T* range and consequently is heavily parameterized. Because these authors do not consider gas-phase compositions, our model cannot be compared with theirs regarding water content in compressed CO_2. Note that we could not reproduce the high-CO_2 concentration data of Gehrig et al. (1986) (close to critical compositions), and consequently, excluded these data from our fits. At elevated temperatures, the effect of dissolved salts on the water solubility in CO_2 is small in comparison to the effect on aqueous CO_2 solubility (Figs. 6 and 7). As evidenced by earlier investigations (Tödheide and Frank 1963; Takenouchi and Kennedy 1965; Gehrig et al. 1986), the presence of dissolved salts significantly raises the critical line of the CO_2–H_2O mixture.

3 Application to the Simulation of CO_2–EGS

Operating enhanced geothermal systems (EGS) with CO_2 instead of water as heat transmission fluid is a novel concept that was originally proposed by Brown (2000). Brown pointed out that CO_2 has attractive properties as an operating fluid for EGS, and could provide storage of greenhouse gases as ancillary benefit. The favorable properties of CO_2 emphasized by Brown include the following:

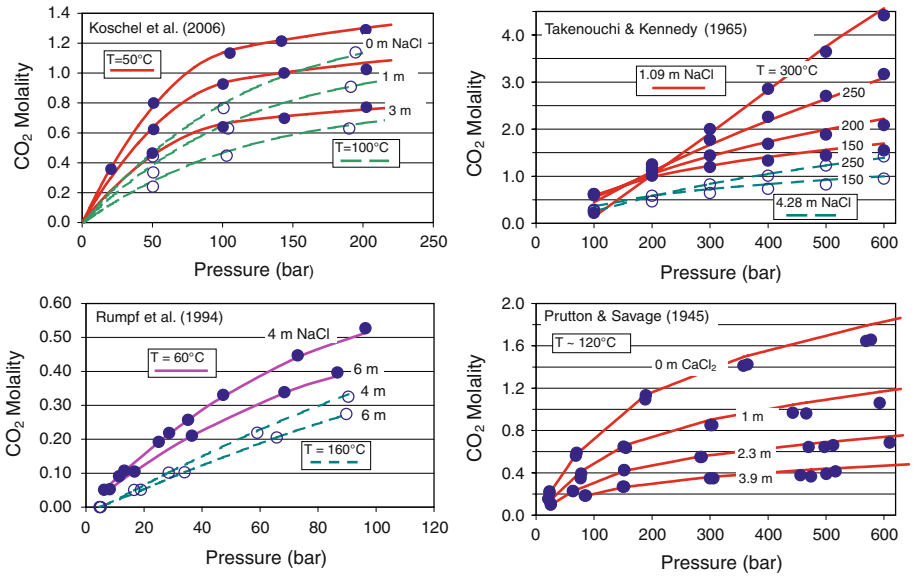

Fig. 4 Solubility of CO_2 in saline solutions: comparison of model results (*lines*) with experimental data (*symbols*) at various temperatures and pressures

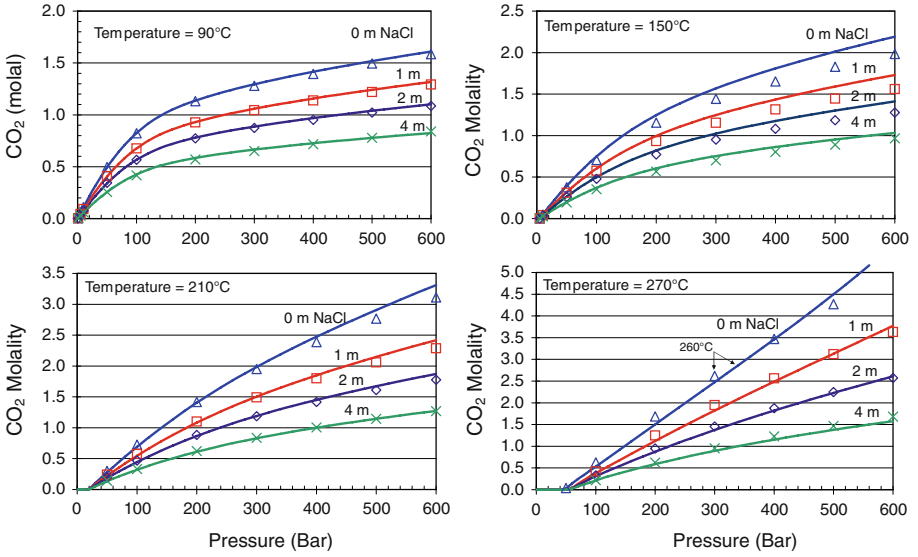

Fig. 5 Computed CO_2 solubility in pure and saline water: Comparison of model results from this study (*lines*) with those of Duan and Sun (2003) (*symbols*)

- Large expansivity would generate large density differences between the cold CO_2 in the injection well and the hot CO_2 in the production well, and would provide buoyancy force that would reduce the power consumption of the fluid circulation system;
- Lower viscosity would yield larger flow velocities for a given pressure gradient; and

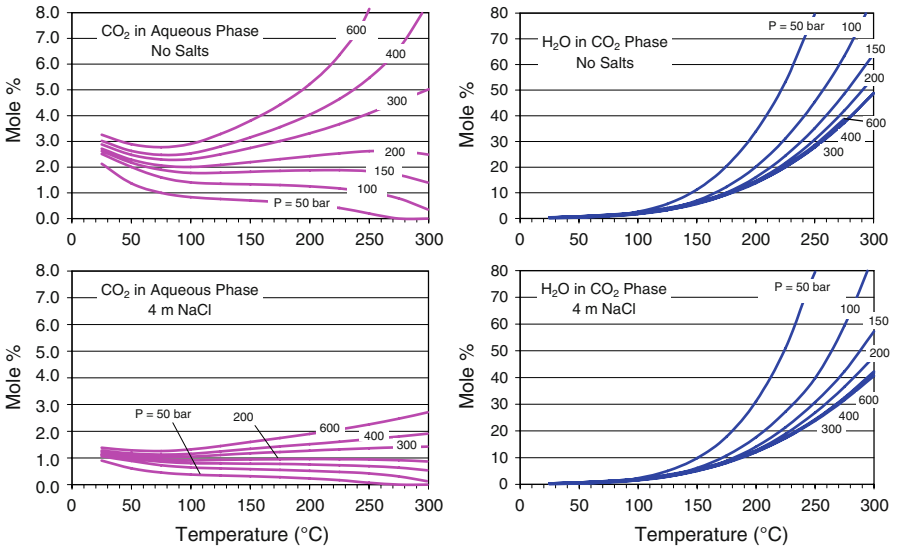

Fig. 6 Computed mutual solubilities of CO_2 and H_2O as a function of temperature at various pressures, for pure water and a 4 molal NaCl solution

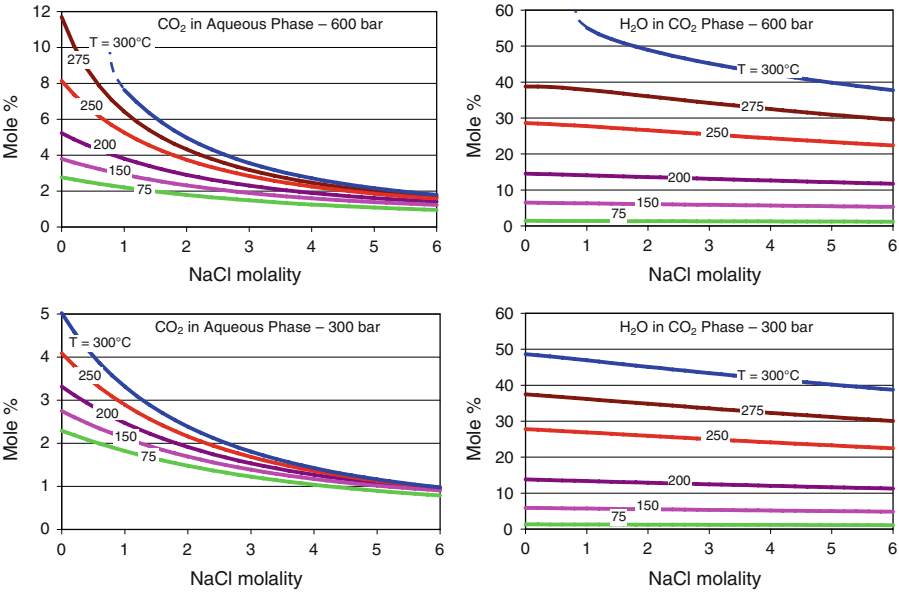

Fig. 7 Computed mutual solubilities of CO_2 and H_2O as a function of salinity between 75 and 300°C at elevated pressures

- CO_2 would be much less effective as a solvent for rock minerals, which would reduce or eliminate scaling problems, such as silica dissolution and precipitation in water-based systems.

Brown also noted the lower mass heat capacity of CO_2 as an unfavorable property, but pointed out that this would be partially compensated by the greater flow capacity of CO_2 due to lower

viscosity. A recent comparison of mathematical models for water- and CO_2-based EGS suggested a potential for substantially larger heat extraction rates for CO_2 as compared to water (Pruess 2006, 2008). Operating EGS with CO_2 may offer large capacity for CO_2 storage as well. Based on observed fluid losses during long-term circulation tests in EGS systems, we estimated that CO_2 could be stored at a rate of 1 kg/s per megawatt (MW) of installed electric generation, corresponding to the CO_2 emissions of 3 MW (electric) of coal-fired generation (Pruess 2006). In order to put these numbers in perspective, consider the first industrial-scale CO_2 geologic storage project at the Sleipner Vest field in the Norwegian sector of the North sea, which has injected approximately 1 million tons of CO_2 per year (31.7 kg/s) into a saline aquifer for over 10 years (Audigane et al. 2007). According to our estimates, CO_2 storage at the same rate as Sleipner could be achieved with a modest-size EGS–CO_2 installation of 30–35 MW electric power.

Initial development of EGS by means of hydraulic and chemical stimulation will result in a reservoir whose pore space will be saturated with aqueous fluids. Operating such a system with CO_2 as heat transmission fluid requires an additional reservoir development step, namely, the removal of the aqueous phase from (at least) the central zone of the EGS system, and its replacement by CO_2. The studies (Pruess 2006, 2008) had compared all-water with all-CO_2 EGS, but had not addressed how an initially water-based system could be converted to operate with CO_2. This issue could not be tackled, because modeling capabilities for water–CO_2 mixtures were limited to temperatures below 110°C. Analyzing this crucial step in the development of EGS with CO_2 requires a capability for modeling the flow of water–CO_2 mixtures over the entire range of temperature conditions, from near-ambient injection temperatures to original reservoir temperatures, and for arbitrary compositions of water–CO_2 mixtures. In this section, we utilize the correlations for phase partitioning between NaCl–brine and CO_2 newly developed in this study for a first exploration of the manner in which continuous circulation of CO_2 will remove water from an EGS.

3.1 Modeling Approach

We consider a five-spot "generic" EGS injection-production system with parameters patterned after the European hot dry rock project at Soultz/France (Gérard et al. 2006). The reservoir is treated as a two-dimensional areal system (Fig. 8), with an initial temperature of 200°C, and similar problem specifications (Table 4) as in Pruess (2006). In Pruess (2006), we had modeled and compared EGS production behavior for (1) water injection into an all-water system, and (2) CO_2 injection into an all-CO_2 system. In contrast, here we model the injection of 100% dry (anhydrous) CO_2 into a reservoir that is all (fresh) water initially. Our focus is on the removal of water by immiscible displacement from CO_2, as well as by evaporation (dissolution) into the flowing CO_2 stream. The EGS reservoir is modeled as a fractured system with three orthogonal fracture sets at $D = 50$-m spacing. The unfractured matrix rock has small but finite porosity and permeability, as appropriate for tight reservoir rocks such as graywacke or granite (Pruess 2002). The MINC approach is used to represent fluid and heat exchange between fractures and rock matrix (Pruess and Narasimhan 1985).

The process considered is injection of CO_2 at a temperature of 20°C with a (downhole) overpressure of 10 bar relative to original reservoir pressure of 200 bar, while fluid production occurs against a downhole pressure of $(200 - 10) = 190$ bar. A key aspect of the behavior of the flow system is two-phase flow of water–CO_2 mixtures in both fractures and matrix rock, driven by externally imposed pressure gradients, as well as by gradients of capillary pressure that evolve in response to increasing gas saturations from CO_2 injection. Information on interfacial tension and capillary pressures between CO_2 and water is available

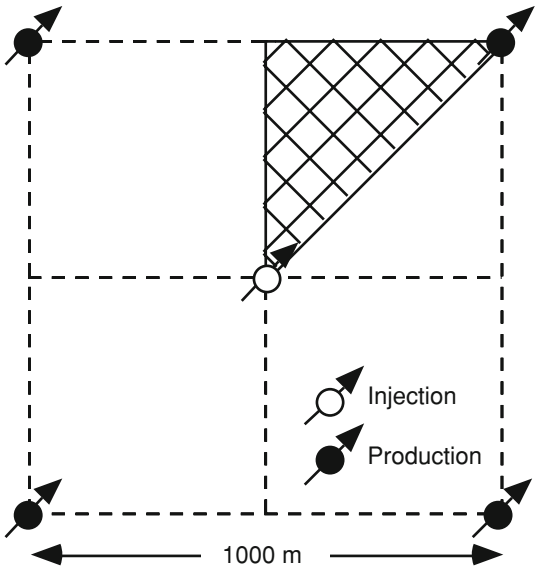

Fig. 8 Five-spot well pattern with computational grid for modeling a 1/8 symmetry domain

only for temperatures below 125°C (Bachu and Bennion 2008; Chiquet et al. 2007). For the simulations performed here, we base the strength coefficient P_0 of capillary pressure (Table 4) on a CO_2-water interfacial tension of $\gamma = 0.028$ N/m, as measured for $T = 50°C$, $P = 200$ bar (Chiquet et al. 2007). Due to continuous injection of dry CO_2, parts of the flow system dry out, necessitating a consistent treatment of capillary pressure for liquid water as liquid saturation $S_l \longrightarrow 0$. We use the approach proposed by Webb (2000) to modify the van Genuchten (1980) capillary pressure function in the dry region, imposing a limiting strength of $P_{cap} = -1,000$ bar as $S_1 \longrightarrow 0$.

The simulations are performed with our general-purpose simulator TOUGH2 (Pruess 2004), using a version of the ECO2N fluid property module for brine–CO_2 mixtures (Pruess and Spycher 2007) that was modified to incorporate the new correlation for brine–CO_2 phase partitioning developed in this article.

3.2 Results

Simulation results are given in Figs. 9 and 10. Initial fluid production in response to CO_2 injection is single-phase water. Breakthrough of CO_2 at the production well occurs after 46 days, and subsequently a two-phase water–CO_2 mixture is produced. Over time, the rate of gas production increases, while aqueous phase production declines, reflecting relative permeability effects as gas saturations in the reservoir increase from continuous CO_2 injection. After 3.9 years of CO_2 injection, aqueous phase production ceases, and subsequently a single-phase stream of supercritical CO_2 is produced. At the time when an aqueous phase ceases to be produced, the produced CO_2 includes approximately 6.4% by weight of dissolved water (Fig. 10). The water content in the produced fluid declines fairly rapidly after aqueous phase production ceases, due to partial reservoir dryout in the fractures, dropping below 1% after 7.4 years. The decline of H_2O concentrations slows over time, dropping below 0.1% after 17.1 years, while at the end of the simulation, after 36.5 years, water content in produced CO_2

Table 4 Parameters for five-spot fractured reservoir

Formation	
Thickness	$H = 305\,\text{m}$
Fracture spacing	$D = 50\,\text{m}$
Relative permeabilities (Corey 1954)	
Liquid $k_{rl} = \hat{S}^4$	$S_{lr} = 0.30$
Gas $k_{rg} = (1 - \hat{S})^2(1 - \hat{S}^2)$	$S_{gr} = 0.05$
where $\hat{S} = (S_l - S_{lr})/(1 - S_{lr} - S_{gr})$	
Capillary pressure (van Genuchten 1980)	
$P_{cap} = -P_0([S_l]^{-1/\lambda} - 1)^{1-\lambda}$	$\lambda = 0.4438$
Parameter	
Strength coefficient for fractures	$P_{0,f} = 0.0416\,\text{bar}$
Strength coefficient for matrix	$P_{0,m} = 6.734\,\text{bar}$
Fracture domain	
Volume fraction	2%
Intrinsic porosity[a]	$\phi_f = 50\%$
Fracture network permeability	$k_f = 50.0 \times 10^{-15}\text{m}^2$
Matrix domain	
Volume fraction	98 %
Intrinsic porosity	$\phi_m = 1\%$
Matrix permeability	$k_m = 1.9 \times 10^{-18}\text{m}^2$
Thermal parameters	
Rock grain density	$\rho_R = 2,650\,\text{kg/m}^3$
Rock specific heat	$c_R = 1,000\,\text{J/kg/°C}$
Rock thermal conductivity	$K = 2.1\,\text{W/m/°C}$
Initial Conditions	
Reservoir fluid	All water
Temperature	$T_{in} = 200°\text{C}$
Pressure	$P_{in} = 200\,\text{bar}$
Production/Injection	
Pattern area	$A = 1\,\text{km}^2$
Injector-producer distance	L = 707.1 m
Injection temperature	$T_{inj} = 20°\text{C}$
Injection pressure (downhole)	$P_{inj} = P_{in} + 10\,\text{bar}$
Production pressure (downhole)	$P_{pro} = P_{in} - 10\,\text{bar}$

[a] we include some wall rock in the definition of the fracture domain

is 0.012%. Almost half of the initial water inventory in the reservoir still remains in place after 36.5 years.

We performed limited sensitivity studies, varying parameters such as strength of capillary pressure, and matrix porosity and permeability. We also ran a simulation that included molecular diffusion of water dissolved in CO_2, and CO_2 dissolved in water. These problem variations did affect quantitative details of reservoir production behavior, but had only limited effects on the water content of produced CO_2. While production of a free aqueous phase from an EGS operated with CO_2 will occur for only a limited time (a few years), we conclude that significant dissolved water will persist in the CO_2 production stream for decades.

An attractive possible design for generating electric power from EGS operated with CO_2 would directly feed the produced CO_2 stream to a turbine, thereby avoiding capital and operating expenses, and heat losses of a heat exchanger. Because our simulations suggest that significant concentrations of dissolved water would persist in the CO_2, it will be necessary to dry the produced fluid upstream of the turbine, akin to removing the "H_2O contaminant," to avoid corrosion from water condensation and carbonic acid formation at the low-P, low-T side of the turbine.

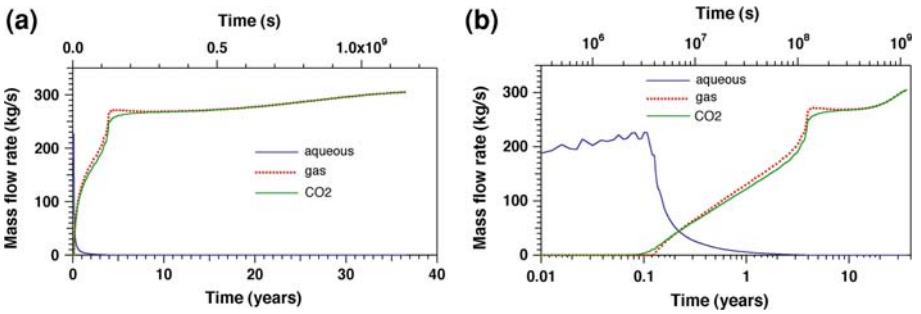

Fig. 9 Simulated production behavior of the EGS system in response to injection of pure CO_2 at constant downhole pressure of 210 bar on linear (**a**) and logarithmic time scales (**b**)

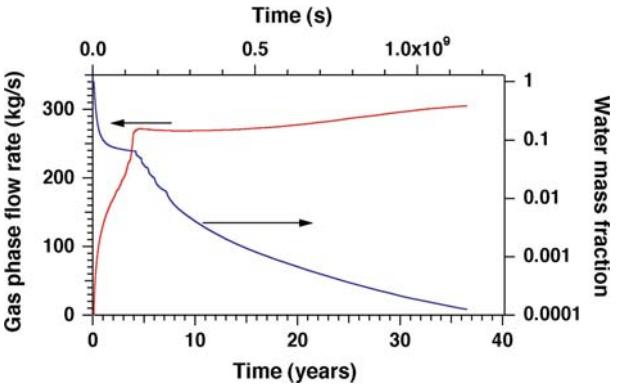

Fig. 10 Simulated rate and composition of produced fluid

4 Summary and Conclusions

Our earlier model for phase partitioning in CO_2–brine mixtures below about 100°C (Spycher et al. 2003) was extended to 300°C for applications relevant to high-temperature CO_2 sequestration and CO_2–EGS systems. The model generally reproduces experimental solubilities within the scatter of available data (Figs. 1 and 2), with an accuracy appropriate for investigating CO_2 and water flows in geologic systems at pressures up to about 600 bar. A noticeable exception is the inaccurate reproduction of water content in CO_2 near the critical line at 300°C above 400 bar (Fig. 2), which should be expected from a relatively simple model like the one presented here. Nevertheless, mutual solubilities are reproduced with RMSD values of about 7% for CO_2 in water and 17% for water in CO_2, the latter, more significant deviation being caused primarily by divergent experimental datasets.

The extended high-temperature model was kept consistent with the original low-temperature model, and was minimally parameterized in an effort to keep it efficient for implementation into numerical multiphase flow models. As such, the mutual solubility model is non-iterative below 99°C, and makes use of a numerically efficient back-substitution method for the iterative approach required at higher temperatures. This is seen as an advantage over other solubility models, which are either heavily parameterized and computationally slow, or not suitable to compute both gas and aqueous phase compositions.

As part of this study, a large amount of experimental data on the solubility of CO_2 in NaCl (primarily) and $CaCl_2$ solutions were regressed to allow the calculation of mutual solubilities of CO_2 and water for saline solutions up to about 6 m NaCl. In doing so, correlations to compute activity coefficients for aqueous CO_2 from ~20 to 300°C and up to 600 bar were presented. These correlations, together with expressions and parameters developed to compute equilibrium constants for aqueous CO_2, are suitable for implementation into other models designed to compute multicomponent geochemical equilibria.

The phase-partitioning correlations developed in this study were implemented into a multiphase flow numerical model to simulate a (hypothetical) CO_2-EGS system, in which dry supercritical CO_2 at 20°C is injected into a 200°C hot-water reservoir. A 2D horizontal numerical mesh was developed, comprising one injection and one production well (representing a 1/8 symmetry domain of a 5-spot well pattern), and a fractured reservoir represented by two continua (fractures and matrix). Simulation results show a declining amount of water and increased CO_2 content in produced fluid, with water production ending after about 4 years. At this point, about 6% (by weight) water remain in the produced single-phase CO_2 stream, decreasing thereafter to <1% after ~7 years, <0.1% after ~17 years, and <0.01% after ~36 years. After this time, almost half of the initial water inventory in the reservoir remains. These results suggest that although water is relatively quickly displaced by the CO_2 plume, significant amounts of water may remain dissolved in the produced CO_2 phase for long periods of time. The presence of water in the CO_2 would have implications not only for the design of heat extraction systems, but would also dictate the amount of reactivity of CO_2 with the reservoir and engineered systems. For these reasons, future assessment of the potential for CO_2-EGS will need to focus not only on flow/recovery issues, but also on the reactivity of CO_2 containing various amounts of water (including dry CO_2) with reservoir rocks and other relevant materials.

Acknowledgments We are grateful to Matthew Reagan for an internal review of this article, as well as to David Kaszuba and two other anonymous reviewers for their review comments. This study was supported by Contractor Supporting Research (CSR) funding from Berkeley Lab, provided by the Director, Office of Science, and by the Zero Emission Research and Technology project (ZERT) under Contract No. DE-AC02-05CH11231 with the U.S. Department of Energy.

Appendix A—Equation of State and Mixing Rules

The following Redlich–Kwong equation of state is used to compute volume (V) as a function of temperature and pressure:

$$P = \left(\frac{RT_K}{V - b_{mix}}\right) - \left(\frac{a_{mix}}{T_K^{0.5} V(V + b_{mix})}\right) \tag{A-1}$$

Equation A-1 is recast as the following cubic expression:

$$V^3 - V^2\left(\frac{RT_K}{P}\right) - V\left(\frac{RT_K b_{mix}}{P} - \frac{a_{mix}}{PT_K^{0.5}} + b_{mix}^2\right) - \left(\frac{a_{mix}\, b_{mix}}{PT_K^{0.5}}\right) = 0 \tag{A-2}$$

Parameters a_{mix} and b_{mix} in Eqs. A-1 and A-2 represent measures of intermolecular attraction and repulsion, respectively, and are computed using the mixing rules described below. Other parameters are as defined earlier. Equation A-2 is solved for the volume of the compressed gas phase (or the stable phase, gas or liquid, below the critical point of CO_2) as described in Spycher et al. (2003).

The mixing rules of Panagiotopoulos and Reid (1986) are applied, as reformulated (equivalent) in Orbey and Sandler (1998):

$$a_{mix} = \sum_{i=1}^{n}\sum_{j=1}^{n} y_i y_j a_{ij} \tag{A-3}$$

$$b_{mix} = \sum_{i=1}^{n} y_i b_i \tag{A-4}$$

with

$$a_{ij} = \sqrt{a_{ii} a_{jj}}(1 - k_{ij}) \tag{A-5}$$

and

$$k_{ij} = K_{ij} y_i + K_{ji} y_j \tag{A-6}$$

Parameters k_{ii} and K_{ii} are always zero (i.e., non-zero values are only for cross-terms) and $K_{ij} \neq K_{ji}$. When K_{ij} and K_{ji} are set to zero, the mixing rules revert to original van der Waals mixing rules. Parameters a_{ii}, b_i, K_{ij}, and K_{ij} are expressed as functions of temperature, $F(T_K)$, in the form:

$$F(T_K) = a + bT_K \tag{A-7}$$

Note, however, that in the low-temperature model, which is implemented in this study at $T < 99°C$, the parameter a_{ij} is not computed using Eq. A-5, and the value of a_{ij} is entered directly as a function of temperature (Eq. A-7). In addition, the assumption is made that $y_{H_2O} = 0$ in the mixing rules and expressions to calculate fugacity coefficients, and therefore a value of a_{H_2O}(a_{ii} for water) is not needed (see Spycher et al. 2003).

The fugacity coefficient, Φ_k, of component k in mixtures with other components i is then calculated with the following equation after Panagiotopoulos and Reid (1986)[2]:

$$\ln(\Phi_k) = \frac{b_k}{b_{mix}}\left(\frac{PV}{RT_K} - 1\right) - \ln\left(P\frac{(V - b_{mix})}{RT_K}\right) + \left(\frac{\sum_{i=1}^{n} y_i(a_{ik}+a_{ki}) - \sum_{i=1}^{n}\sum_{j=1}^{n} y_i^2 y_j (k_{ij}-k_{ji})\sqrt{a_i a_j} + x_k \sum_{i=1}^{n} x_i (k_{ki}-k_{ik})\sqrt{a_i a_k}}{a_{mix}} - \frac{b_k}{b_{mix}}\right) \times \left(\frac{a_{mix}}{b_{mix} RT_K^{1.5}}\right)\ln\left(\frac{V}{V + b_{mix}}\right) \tag{A-8}$$

[2] In the denominator of the fourth term of Eq. A-8, T_K is raised to the power 1.5, whereas it is not in the equation given by Panagiotopoulos and Reid (1986). This is because these authors use a form of the Redlich–Kwong equation of state that does not include a $T_K^{0.5}$ term in the denominator of its second term, as it does in Eq. A-1.

Appendix B—Extension for Saline Solutions

Equations 8 and 9 are replaced by (Spycher and Pruess 2005)

$$y_{H_2O} = A(1 - x_{CO_2} - x_{salt}) \tag{B-1}$$

$$x_{CO_2} = B'(1 - y_{H_2O}) \tag{B-2}$$

where A and B' are defined by Eqs. 10 and 17, respectively. The salt mole fraction, x_{salt}, is defined on the basis of a fully dissociated salt, with

$$x_{salt} = \frac{\upsilon m_{salt}}{55.508 + \upsilon m_{salt} + m_{CO_2(aq)}} \tag{B-3}$$

$$m_{CO_2} = \frac{x_{CO_2} 55.508}{x_{H_2O}} \tag{B-4}$$

$$x_{H_2O} = 1 - x_{CO_2} - x_{salt} \tag{B-5}$$

where υ is the stoichiometric number of ions contained in the dissolved salt (i.e., 2 for NaCl, 3 for $CaCl_2$, etc.) Alternatively, we can also write

$$m_{CO_2} = \frac{x_{CO_2}(\upsilon m_{salt} + 55.508)}{(1 - x_{CO_2})} \tag{B-6}$$

Equations B-1 and B-2 are solved by substitution, yielding (Spycher and Pruess 2005)

$$y_{H2O} = \frac{(1 - B')55.508}{(1/A - B')(\upsilon\ m_{salt} + 55.508) + \upsilon\, m_{salt} B'} \tag{B-7}$$

Therefore, for saline systems, Eqs. B-7 and B-2 replace Eqs. 16 and 9, respectively, developed for the pure-water system.

References

Audigane, P., Gaus, I., Czernichowski-Lauriol, I., Pruess, K., Xu, T.: Two-dimensional reactive transport modeling of CO_2 injection in a saline aquifer at the sleipner site, North Sea. Am. J. Sci. **307**, 974–1008 (2007)

Bachu, S., Bennion, B.: Effects of in-situ conditions on relative permeability characteristics of CO_2-brine systems. Environ. Geol. **54**(8), 1707–1752 (2008)

Bando, S., Takemura, F., Nishio, M., Hihara, E., Akai, M.: Solubility of CO_2 in aqueous solutions of NaCl at 30 to 60°C and 10 to 20 MPa. J. Chem. Eng. Data **48**, 576–579 (2003)

Blencoe, J.G., Naney, M.T., Anovitz, L.: The CO_2–H_2O system: III. A new experimental method for determining liquid-vapor equilibria at high supercritical temperatures. Am. Mineral. **86**, 1100–1111 (2001)

Brown, D.W.: A hot dry rock geothermal energy concept utilizing supercritical CO_2 instead of water. Proceedings, twenty-fifth workshop on geothermal reservoir engineering, Stanford University, January 2000, pp. 233–238

Carlson, H., Colburn, A.P.: Vapor-liquid equilibria of nonideal solutions: utilization of theoretical methods to extend data. Ind. Eng. Chem. **34**, 581–589 (1942)

Chiquet, P., Daridon, J.L., Broseta, D., Thibeau, S.: CO_2/water interfacial tensions under pressure and temperature conditions of CO_2 geological storage. Energy Convers. Manage. **48**, 736–744 (2007)

Coan, C.R., King, A.D. Jr.: Solubility of water in compressed carbon dioxide, nitrous oxide, and ethane. Evidence for hydration of carbon dioxide and nitrous oxide in the gas phase. J. Am. Chem. Soc. **93**, 1857–1862 (1971)

Corey, A.T.: The interrelation between gas and oil relative permeabilities. Producers Monthly, pp. 38–41, November 1954

Cramer, S.D.: The solubility of methane, carbon dioxide, and oxygen in brines from 0 to 300°C. Report of investigations 8706, U.S. Department of the Interior, Bureau of Mines (1982)

Denbigh, K.: The principles of chemical equilibrium, 4th ed. Cambridge University Press, 494 pp. (1983)
Doherty, J.: PEST—model-independent parameter estimation. Watermark Numerical Computing, Corinda 4075, Brisbane, Australia (2008) http://www.sspa.com/pest/
Drummond, S.E.: Boiling and mixing of hydrothermal fluids: chemical effects on mineral precipitation. Ph.D. thesis, Pennsylvania State University (1981)
Duan, Z., Sun, R.: An improved model calculating CO_2 solubility in pure water and aqueous NaCl solutions from 257 to 533 K and from 0 to 2000 bar. Chem. Geol. **193**, 257–271 (2003)
Gilfillan, S.M.V., Ballentine, C.J., Holland, G., Blagburn, D., Sherwood Lollar, B., Stevens, S., Schoell, M., Cassidy, M.: The noble gas geochemisry of natural CO_2 gas reservoirs from the Coloradeau Plateau and Rocky Montain provinces, USA. Geochimica Et Cosmochimica Acta **72**, 1174–1198 (2008)
Fenghour, A., Wakeham, W.A., Watson, J.T.R.: Densities of (water + carbon dioxide) in the temperature range 415 K to 700 K and pressures up to 35 MPa. J. CHem. Thermodynamics **28**, 433–446 (1996)
Fouillac, C., Sanjuan, B., Gentier, S., Czernichowski-Lauriol, I.: Could sequestration of CO_2 be combined with the development of enhanced geothermal systems? In: Paper presented at the Third Annual Conference on Carbon Capture and Sequestration, Alexandria, Virginia, May 3–6, 2004
Gehrig, M., Lentz, H., Frank, E.U.: The system water-carbon dioxide-sodium chloride to 773 K and 300 MPa. Ber. Bunsenges. Phys. Chem. **90**, 525–533 (1986)
Gérard, A., Genter, A., Kohl, T., Lutz, P., Rose, P., Rummel, F.: The deep EGS (Enhanced Geothermal System) project at Soultz-sous-Forets (Alsace, France). Geothermics **35**(5-6), 473–483 (2006)
Gillepsie, P.C., Wilson, G.M.: Vapor-liquid and liquid-liquid equilibria: water-methane, water-carbon dioxide, water-hydrogen sulfide, water-npentane, water-methane-npentane. Research report RR-48, Gas Processors Association, Tulsa Okla, April (1982)
Giorgis, T., Carpita, T., Batistelli, A.: 2D modeling of salt precipitation during injection of dry CO_2 in a depleted gas reservoir. Energy Conserv. Manage. **48**, 1816–1826 (2007)
Goyal, K.: Injection recovery factors in various areas of the Southeast Geysers, California. Geothermics **24**, 167–186 (1995)
Hurter, S., Labregere, D., Berge, J.: Simulations of dry-out and halite precipitation due to CO_2 injection. Geochimica Et Cosmochimica Acta **71**, A426–A426 (2007)
Hu, J., Duan, Z., Zhu, C., Chou, I.-M.: PVTx properties of the CO_2–H_2O and CO_2–H_2O-NaCl systems below 647 K: assessment of experimental data and thermodynamic models. Chem. Geol. **238**, 249–267 (2007)
IPCC: Carbon dioxide capture and storage In: Metz, B., Davidson, O., de Coninck, H., Loos, M., Meyer, L. (eds.) Prepared by Working Group III of the Intergovernmental Panel on Climate Change, Cambridge University Press, 431 pp. (2005)
IPCC: Climate change 2007: synthesis report. Contributions of working groups I, II, and III to the fourth assessment report of the intergovernmental panel on climate change. In: Core Writing Team, Pachauri, R.K., Reisinger, A. (eds.) Intergovernmental Panel on Climate Change, c/o World Meteorological Organization, Geneva, Switzerland, 104 pp. (2008)
Kaszuba, J.P., Janecky, D.R., Snow, M.G.: Carbon dioxide sequestration processes in a model brine aquifer at 200°C and 200 bars: implications for geologic sequestration of carbon. Applied Geochemistry **18**:1065–1080 (2003)
Kiepe, J., Horstmann, S., Fisher, K., Gmehling, J.: Experimental determination and prediction of gas solubility data for $CO_2 + H_2O$ mixtures containing NaCl or KCl at temperatures between 313 and 393 K and pressures up to 10 MPa. Ind. Eng. Chem. Res. **41**, 4393–4398 (2003)
Koschel, D., Coxam, J.-Y., Rodier, L., Majer, V.: Enthalpy and solubility of CO_2 in water and NaCl(aq) at conditions of interest for geological sequestration. Fluid Phase Equilibria **247**, 107–120 (2006)
Lin, H., Fujii, T., Takisawa, R., Takahashi, T., Hashida, T.: Experimental evaluation of interactions in supercritical CO_2/water/rock mineral system under geologic CO_2 sequestration conditions. J. Mater. Sci. **43**, 2307–2315 (2008)
Malinin, S.D., Kurovskaya, N.A.: Investigations of CO_2 solubility in a solution of chlorides at elevated temperatures and pressures of CO_2. Geokhimiya **4**, 547–551 (1975)
Malinin, S.D., Savelyeva, N.I.: The solubility of CO_2 in NaCl and $CaCl_2$ solutions at 25, 50, and 75°C under elevated CO_2 pressures. Geokhimiya **6**, 643–653 (1972)
Malinin, S.D.: The system water-carbon dioxide at high temperatures and pressures. Geokhimiya **3**, 235–245 (1959)
Markham, A.E., Kobe, K.A.: The solubility of carbon dioxide and nitrous oxide in aqueous salt solutions. J. Am. Chem. Soc. **63**, 449–454 (1941)
Müller, G., Bender, E., Maurer, G.: Das Dampf-Flüssigkeitsgleichgewicht des ternären Systems Ammoniak-Kohlendioxid-Wasser bei hohen Wassergehalten im Bereich zwischen 373 und 473 Kelvin. Berichte der Bunsen-Gesellshaft für Physikalische Chemie **92**, 148–160 (1988)
MIT (ed.): *The Future of Geothermal Energy*. (Massachusetts Institute of Technology, Cambridge, MA 2006)

Moore, J. Adams, Allis, R., Lutz, S., Rauzi, S.: Mineralogical and geochemical consequences for the long-term presence of CO_2 in natural reservoirs: an example from the Spingville-St. Johns Field, Arizona, and New Mexico, U.S.A.. Chem. Geol. **217**, 365–385 (2005)

Nickalls, R.W.D.: A new approach to solving the cubic: Cardan's solution revealed. Math. Gaz. **77**, 354–359 (1993)

Nighswander, J.A., Kalogerakis, N., Mehotra, A.K.: Solubilities of carbon dioxide in water and 1 wt% NaCl solution at pressures up to 10 MPa and temperatures from 80 to 200°C. C. J. Chem. Eng. Data **34**, 355–360 (1989)

Orbey, H., Sandler, S.I.: Modeling Vapor-Liquid Equilibria: Cubic Equations of State and their Mixing Rules. Cambridge University Press (1998)

Palandri, J., Rosenbauer, R.J., Kharaka, Y.K.: Ferric iron in sediments as a novel CO_2 mineral trap: CO_2–SO_2 reaction with hematite. Appl. Geochem. **20**, 2038–2048 (2005)

Panagiotopoulos, A.Z., Reid, R.C.: New mixing rules for cubic equations of state for highly polar asymmetric mixtures. ACS Symposium Series 300: American Chemical Society, Washington, D.C., pp. 571–582 (1986)

Pruess, K.: Numerical simulation of multiphase tracer transport in fractured geothermal reservoirs. Geothermics **31**, 475–499 (2002)

Pruess, K.: The TOUGH codes—a family of simulation tools for multiphase flow and transport processes in permeable media. Vadose Zone J. **3**, 738–746 (2004)

Pruess, K.: Enhanced geothermal systems (EGS) using CO_2 as working fluid—a novel approach for generating renewable energy with simultaneous sequestration of carbon. Geothermics **35**(4), 351–367 (2006)

Pruess, K.: On production behavior of enhanced geothermal systems with CO_2 as working fluid. Energy Convers. Manage. **49**, 1446–1454 (2008)

Pruess, K., Narasimhan, T.N.: A practical method for modeling fluid and heat flow in fractured porous media. Soc. Pet. Eng. J. **25**(1), 14–26 (1985)

Pruess, K., Spycher, N.: ECO2N—a fluid property module for the TOUGH2 code for studies of CO_2 storage in saline aquifers. Energy Convers. Manage. **48**(6), 1761–1767 (2007)

Pruess, K., Müller, N.: Formation dry-out from CO_2 injection into saline aquifers: 1. Effects of solids precipitation and their mitigation. Water Resour. Res. **45**, W03402, doi:10.1029/2008WR007101 (2009)

Prutton, C.F., Savage, R.L.: The solubility of carbon dioxide in calcium chloride-water solutions at 75, 100, 120°C and high pressures. J. Am. Chem. Soc. **67**, 1550–1554 (1945)

Regnault, O., Lagneau, V., Catalette, H., Schneider, H.: Etude expérimentale de la réactivité du CO_2 supercritique vis-à-vis de phases minérales pures Implications pour la séquestration géologique de CO_2. Comptes Rendus Geosci. **337**, 1331–1339 (2005)

Rimmelé, G., Barlet-Gouédard, V., Porcherie, O., Goffé, B., Brunet, F.: Heterogeneous porosity distribution in Portland cement exposed to CO_2-rich fluids. Cem. Concr. Res. **38**, 1038–1048 (2008)

Rosenbauer, R.J., Koksalan, T., Palandri, J.L.: Experimental investigation of CO_2-brine-rock interactions at elevated temperature and pressure: Implications for CO_2 sequestration in deep-saline aquifers. Fuel Process. Technol. **86**, 1581–1597 (2005)

Rumpf, B., Nicolaisen, H., Ocal, C., Maurer, G.: Solubility of carbon dioxide in aqueous solutions of sodium chloride: experimental results and correlation. J. Solut. Chem. **23**, 431–448 (1994)

Sako, T., Sugeta, T., Nakazawa, N., Obuko, T., Sato, M., Taguchi, T., Hiaki, T.: Phase equilibrium study of extraction and concentration of furfural produced in reactor using supercritical carbon dioxide. J. Chem. Eng. Jpn. **24**, 449–454 (1991)

Shagiakhmetov, R.A., Tarzimanov, A.A.: Deposited document SPSTL 200 khp-D 81-1982 (1981). Summarized in: Sharlin, P.: Carbon Dioxide in Water and Aqueous Electrolyte Solutions. Solubility Data Series, vol. 62, 383 pp. International Union of Pure and Applied Chemistry, Oxford University Press (1996)

Span, R., Wagner, W.: A new equation of state for carbon dioxide covering the fluid region from the triple-point temperature to 1100 K at pressures up to 800 MPa. J. Phys. Chem. Ref. Data **25**(6), 1509–1596 (1996)

Spycher, N., Pruess, K.: Mixtures in the geological sequestration of CO_2. II. Partitioning in chloride brines at 12–100°C and up to 600 bar. Geochimica Et Cosmochimica Acta **69**, 3309–3320 (2005)

Spycher, N., Pruess, K., Ennis-King, J.: CO_2–H_2O Mixtures in the geological sequestration of CO_2. I. Assessment and calculation of mutual solubilities from 12 to 100°C and up to 600 bar. Geochimica Et Cosmochimica Acta **67**, 3015–3031 (2003)

Stark, M.A., Box, W.T. Jr., Beall, J.J., Goyal, K.P., Pingol, A.S.: The Santa Rosa–Geysers recharge project, Geysers geothermal field, California, USA. Proceedings, file 2420.pdf, World Geothermal Congress, Antalya, Turkey, April 2005

Suto, Y., Liu, L., Yamasaki, N., Hashida, T.: Initial behavior of granite in response to injection of CO_2-saturated fluid. Appl. Geochem. **22**, 202–218 (2007)

Takenouchi, S., Kennedy, G.C.: The binary system H_2O–CO_2 at high temperatures and pressures. Am. J. Sci. **262**, 1055–1074 (1964)

Takenouchi, S., Kennedy, G.C.: The solubility of carbon dioxide in NaCl solutions at high temperatures and pressures. Am. J. Sci. **263**, 445–454 (1965)

Tödheide, K., Frank, E.U.: Das Zweiphasengebiet und die kritische Kurve im System Kohlendioxid-Wasser bis zu Drucken von 3500 bar. Z. Phys. Chemie, Neue Folge **37**, 387–401 (1963)

van Genuchten, M.Th.: A closed-form equation for predicting the hydraulic conductivity of unsaturated soils. Soil Sci. Soc. Am. J. **44**, 892–898 (1980)

Vorholz, J., Harismiadis, V.I., Rumpf, B., Panagiotopoulos, A.Z., Maurer, G.: Vapor + liquid equilibrium of water, carbon dioxide, and the binary system, water + carbon dioxide, from molecular simulation. Fluid Phase Equilibria **170**, 203–234 (2000)

Wagner, W., Pruss, A.: The IAPW formulation 1995 for the thermodynamic properties of ordinary water substance for general scientific use. J. Phys. Ref. Data **31**, 387–535 (2002)

Webb, S.W.: A simple extension of two-phase characteristic curves to include the dry region. Water Resour. Res. **36**(6), 1425–1430 (2000)

Wiebe, R., Gaddy, V.L.: The solubility in water of carbon dioxide at 50, 75, and 100°, at pressures to 700 atmospheres. J. Am. Chem. Soc. **61**, 315–318 (1939)